JOURNAL OF CATALYSIS **163,** 28–37 (1996)
ARTICLE NO. 0302

Structure of Oxidic NiMo/SiO_2 Hydrotreating Catalyst Precursors

L. Medici and R. Prins[1]

Laboratorium für Technische Chemie, Eidgenössische Technische Hochschule, CH-8092 Zürich, Switzerland

Received October 30, 1995; revised March 18, 1996; accepted April 24, 1996

The structures of Ni and Mo in dried, but not calcined, oxidic NiMo/SiO_2 hydrotreating catalyst precursors and in the corresponding impregnation solutions were analyzed by means of UV–VIS, Raman, infrared, and X-ray absorption spectroscopies as a function of the impregnation order of the Ni and Mo salts and of the addition of the chelating agent nitrilotriacetic acid (NTA) to the impregnation solutions. The Ni ions in the impregnation solutions which contained Ni, Mo, and NTA, and in the corresponding dried catalyst precursors, were preferentially complexed with NTA. As a consequence of the Ni : Mo : NTA = 0.5 : 1 : 1 molar ratios, Mo was present in about equal amounts as the $[MoO_3(NTA)]^{3-}$ complex and as well-dispersed molybdates, grafted through Si–O–Mo bonds to the support. In NiMo/SiO_2 samples prepared by sequential impregnation with the Mo salt and Ni in the absence of NTA, all Mo was present as well-dispersed polymolybdate grafted on the support after drying only without calcination. When the impregnation order was reversed, $Ni(OH)_2$ crystallites were formed on the surface of SiO_2, onto which MoO_4^{2-} ions attached during the second impregnation.

INTRODUCTION

Hydrotreating catalysts contain sulfides of molybdenum and cobalt or nickel as the active materials, often also promoters such as fluorine and phosphorus, and almost exclusively γ-Al_2O_3 as support (1, 2). Silica-supported catalysts, prepared by conventional pore-filling impregnation, calcination, and sulfidation, have a very poor hydrotreating activity compared to the γ-Al_2O_3-supported counterparts (3). This is usually ascribed to a low dispersion of the molybdenum and cobalt or nickel oxides on SiO_2 (and consequently also of the active sulfides), because of weak interactions with the support (3, 4). By adding chelating molecules like ethylenediaminetetraacetic acid (H_4EDTA, $(HOOCCH_2)_2NCH_2CH_2N(CH_2COOH)_2$) or nitrilotriacetic acid (H_3NTA, $N(CH_2COOH)_3$) to the impregnation solution, it has proved possible, however, to prepare SiO_2-supported hydrotreating catalysts which have a similar activity in the hydrotreatment of heavy gasoil as the commercial γ-Al_2O_3 supported counterparts (3). In some publications it has been claimed that even more active catalysts can be prepared following this recipe (4–8). The presence of an organic complexing agent and the elimination of the calcination of the oxidic precursor seem to be the two main differences between a good and a poor SiO_2-supported catalyst.

This and the succeeding paper (9) deal with the explanation for the high hydrotreating activity of SiO_2-supported hydrotreating catalysts prepared by the addition of NTA to the impregnating solutions. In this first paper the elucidation of the structures of the Ni and Mo complexes in the impregnation solutions and in the impregnated and dried (but not calcined) catalyst precursors will be presented. In the succeeding paper, the sulfidation of the NTA-containing catalyst precursors and the structures and activities of the resulting sulfidic hydrotreating catalysts will be described.

EXPERIMENTAL

The pore volume impregnation method was used to prepare the catalysts. The impregnation solutions which contained the chelating ligand NTA were prepared following the recipe of the European patent application 0.181.035 (3). In 15 ml of a 25% aqueous NH_3 solution (Fluka, puriss. p.a.), 4.78 g H_3NTA (25 mmol, Fluka, puriss. p.a.) was slowly dissolved under vigorous stirring and cooling in an ice bath. Then 3.60 g MoO_3 powder (25 mmol, Fluka, puriss. p.a.) was added. The mixture was refluxed and the MoO_3 dissolved. After cooling to ca. 333 K, 3.64 g $Ni(NO_3)_2 \cdot 6H_2O$ (12.5 mmol, Fluka, purum p.a.) were added and dissolved. The color of the solution turned from transparent to blue or ultramarine after this step, depending on the pH. Finally, the pH was adjusted at 7.5 and the solutions were diluted to 25 ml with H_2O.

Some NiMo/SiO_2 catalysts were made by the classic double impregnation procedure, with either the impregnation with the Ni solution as the first step (denoted by Ni first) or with the Mo solution as the first step (Mo first). The impregnation solutions were prepared by dissolving an appropriate amount of $Ni(NO_3)_2 \cdot 6H_2O$ (Fluka, purum p.a.) or $(NH_4)_6Mo_7O_{24} \cdot 4H_2O$ (Merck, p.a.) in a volume of water approximately corresponding to the pore volume of the support. Unless specified otherwise, the pH of the

[1] E-mail: prins@tech.chem.ethz.ch.

0021-9517/96 $18.00

impregnation solutions was adjusted at 7.5 with diluted NH_3 (ca. 1 mol/l) or HNO_3 (ca. 1 mol/l). Co-impregnated NiMo/SiO_2 catalysts were prepared with a solution containing both metal salts, prepared by sequential dissolution of $(NH_4)_6Mo_7O_{24} \cdot 4H_2O$ followed by $Ni(NO_3)_2 \cdot 6H_2O$ in a ca. 8 mol/l NH_3 solution made by partial titration of 25% aqueous NH_3 with concentrated HNO_3. The pH was then adjusted at 8.5.

Prior to impregnation, the γ-Al_2O_3 (Condea Chemie) and SiO_2 (C560 Chemie Uetikon) supports were crushed, sieved to 125–250 mm fractions and dried overnight in an oven at 393 K. The BET surface areas of γ-Al_2O_3 and SiO_2 were 235 and 410 m^2/g and the BET pore volumes were 0.56 and 0.8 ml/g, respectively. After impregnation, all catalysts were dried in air at 393 K during 12 h (heating rate 1 K/min). Prior to cooling to room temperature, a calcination at 673 K during 2 h (heating rate 6 K/min) was performed on some samples. As proposed in the European patent application (3), all catalysts to which NTA was added were synthesized by co-impregnation of the three components (Ni, Mo, and NTA) and not calcined, in order to avoid the decomposition of the organic molecules and the complexes. The Mo loading was about constant within each series of catalysts: 6.9–7.9 wt% on SiO_2 and 5.0–5.6 wt% on γ-Al_2O_3. All catalysts discussed in this paper are presented in Table 1.

UV–VIS reflectance measurements of the catalysts were carried out on a Perkin Elmer Lambda 16 spectrometer equipped with an integration sphere that allowed measurements in the reflection mode. $BaSO_4$ (Fluka, purum p.a.) was used as a reference. Measurements of solutions were performed in 1-cm quartz cells.

The Raman measurements were performed on a Dilor XY 800 spectrometer equipped with a double monochromator and a CCD camera detector (resolution 1.5 cm^{-1}). An Ar^+ laser (514.5 nm) was used and care was taken that the samples did not overheat. The data acquisition range extended from 130 to 1100 cm^{-1} and the laser beam was focused on the external surface of the spherical quartz sample holder. Five spectra accumulations were averaged and the integration time was chosen between 13 and 20 s to avoid saturation of the CCD detector.

The IR measurements were performed on a Mattson Galaxy 6020 FT-IR spectrometer in transmission mode, with KBr beamsplitter and DTGS detector. For all samples, 32 scans were collected. The sample wafers contained 5% catalyst diluted with KBr (Merck, p.a.) and weighed about 100 mg. As reference a dry KBr pellet was used.

The EXAFS (extended X-ray absorption fine structure) spectra were obtained at the SRS in Daresbury (UK) on stations 8.1 and 9.2. Details regarding the EXAFS measurements and data analysis were published previously (5–7). The experimental Mo–Mo EXAFS contribution in MoS_2 was taken as reference for the second shell Mo–Mo coordination in the oxidic catalysts; for the Ni–Ni contribution we used the Ni–Ni coordination in NiO, while the Mo–Ni contribution in $((C_6H_5)_4P)_2Ni(MoS_4)_2$ was used for the Mo–Ni coordination. For the second shell Mo–Si contribution a theoretical reference was calculated with the FEFF method (10). The Ni *K*-edge spectra which were acquired on station 8.1 were of a substantially better quality than those measured on station 9.2. The signal-to-noise ratio of the former was still good around 13 $Å^{-1}$, whereas the latter had to be truncated at 11 $Å^{-1}$. Ni *K*-edge spectra of an acid and a basic Ni : Mo : NTA = 0.5 : 1 : 1 solution, free of NH_3 and NH_4^+, were measured at room temperature. These solutions were contained in a 1.5 mm thick stainless steel cell, equipped with capton windows.

TABLE 1

Ni–Mo–NTA and Ni–Mo Catalysts Supported on SiO_2 and γ-Al_2O_3

	Atomic ratio			Loading		
Support	Ni	Mo	NTA	Ni (%)	Mo (%)	NTA (%)
SiO_2	0	1	0	0	6.9	0
	0	1	1	0	7.9	15.7
	0.3	1	1	1.4	7.9	15.7
	0.5	1	1	2.3	7.5	15.0
	1	1	1	4.6	7.5	14.9
	1	0	1	4.6	0	15.0
	1	0	0	2.6	0	0
	0.5	1	0	2.2	7.5	0
Al_2O_3	0	1	1	0	5.2	10.4
	0.3	1	1	1.0	5.4	10.7
	0.5	1	1	1.7	5.6	11.1
	1	1	1	3.1	5.0	10.0
	1	0	1	3.0	0	9.9

RESULTS

Impregnating Solutions

An extensive amount of literature is available on the stability of Mo(VI) and Ni^{2+} complexes in aqueous solution (11–15). This cumulated knowledge allows one to predict which Mo and Ni species will be present in solutions containing NH_3 and NTA as a function of pH. Figure 1a shows that solid MoO_3 should dissolve around pH = 2 and successively form more and more deprotonated $MoO_7O_{24-n}(OH)^{(6-n)-}$ species at increasing pH, until eventually MoO_4^{2-} forms above pH = 6 (11). The Raman spectra of 1 molar Mo solutions at pH = 5.5 and 8.8 (Fig. 2, spectra I and VI) are indeed in accordance with those of $Mo_7O_{24}^{6-}$ and MoO_4^{2-}, respectively, as published in the literature (16). In the presence of one equivalent of NTA, the equilibrium conditions change dramatically (Fig. 1b). Between pH = 2 and 9, the most abundant species is $[MoO_3(NTA)]^{3-}$, and MoO_4^{2-} is the major species above pH = 9 only (11–13). The Raman spectra of a 1-molar solution of Mo and NTA (1 : 1)

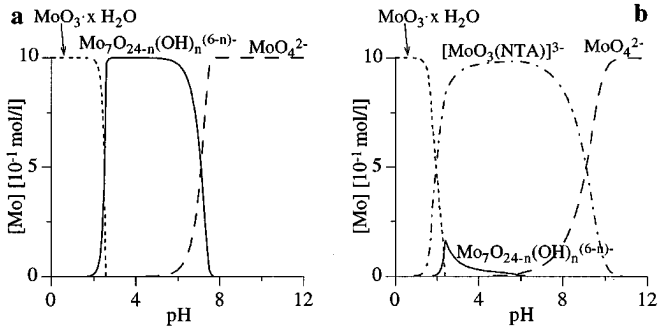

FIG. 1. Thermodynamic predictions of the Mo species ($[Mo]_{tot} =$ 1 mol/l) in aqueous solution as a function of the pH, (a) without and (b) with one NTA equivalent.

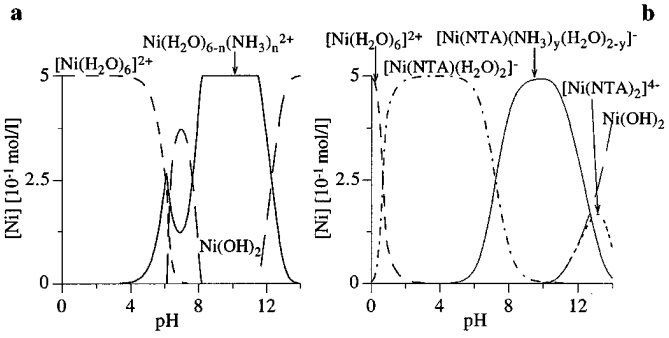

FIG. 3. Thermodynamic predictions of the Ni species ($[Ni]_{tot} =$ 0.5 mol/l) in a 5 mol/l ammonia solution as a function of the pH, (a) without and (b) with one NTA equivalent.

confirmed that at high pH MoO_4^{2-} is present (Fig. 2, spectra IV and V), while at pH = 6 a spectrum appeared (Fig. 2, spectrum III) which is different from those of MoO_4^{2-} and $Mo_7O_{24}^{6-}$ and should, according to Fig. 1b, be due to the presence of the $[MoO_3(NTA)]^{3-}$ complex.

In an aqueous Ni-containing solution, $[Ni(H_2O)_6]^{2+}$ species dominate at low pH. The addition of ammonia leads to $[Ni(NH_3)_6]^{2+}$ species at moderately high pH, and solid $Ni(OH)_2$ around pH = 7 and above pH = 12 (Fig. 3a) (12, 14). With increasing pH, the water ligands in the $[Ni(H_2O)_6]^{2+}$ complex are successively substituted by ammonia. In the presence of one equivalent of NTA, the dominant species is $[Ni(NTA)(H_2O)_2]^-$ over a broad pH-range (Fig. 3b) (12, 14). The addition of NH_3 induces the exchange of NH_3 against H_2O in the $[Ni(NTA)(H_2O)_2]^-$ complex:

$$[Ni(NTA)(H_2O)_2]^- + y\ NH_3 \rightleftharpoons [Ni(NTA)(H_2O)_{2-y}(NH_3)_y]^- + y\ H_2O$$

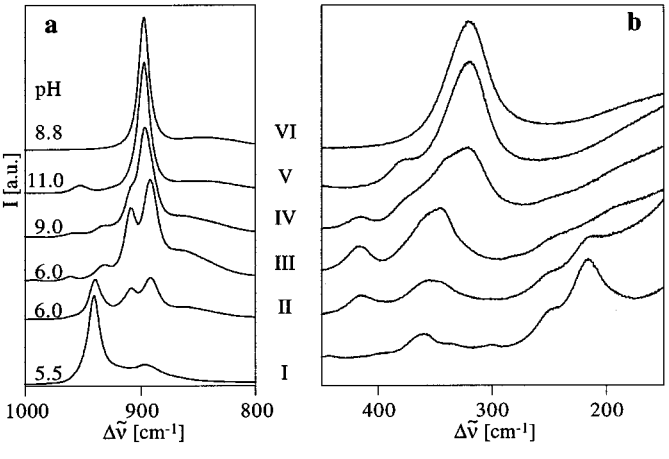

FIG. 2. Raman spectra of aqueous Mo–NTA (1:1) solutions at different pH (III, IV, V), compared with those of $(NH_4)_6Mo_7O_{24}$ (I), Ni–Mo–NTA (0.5:1:1) (II), and Na_2MoO_4 (VI) solutions. In all cases $[Mo]_{tot} = 1$ mol/l.

The UV–VIS absorption spectra of Ni ions in solution are very sensitive to the Ni coordination, and the replacement of H_2O by NH_3 ligands in the $[Ni(NTA)(H_2O)_2]^-$ complex can be clearly distinguished (Fig. 4 and Ref. (17)). UV–VIS measurements showed that at pH = 6 the above NH_3–H_2O exchange equilibrium is at the left (because NH_3 is removed from solution by H^+), while at pH = 9 it has shifted to the right. They also proved that for Ni/NTA ≤ 1 all Ni ions in solution are complexed by NTA ligands. Depending on the NH_3 concentration and pH, $[Ni(NTA)(H_2O)_2]^-$, $[Ni(NTA)(H_2O)(NH_3)]^-$, $[Ni(NTA)(NH_3)_2]^-$, and $[Ni(NTA)_2]^{4-}$ complexes are present in different amounts. At a Ni/NTA = 1 ratio, the $[Ni(NTA)_2]^{4-}$ complex is present above pH = 10, while for Ni/NTA = 0.5 this complex is the dominant Ni species even under neutral conditions.

Thermodynamic predictions (11–15) for the species present in a solution containing Ni, Mo, and NTA in the molar ratio 0.5:1:1 at a total Mo concentration of 1 mol/l are presented in Fig. 5. Since only one equivalent of NTA is available for 0.5 equivalent of Ni and one equivalent of Mo, and since Ni ions can bind one or two NTA ligands, the question arises as to which cation binds NTA more strongly and at which pH. The published equilibrium constants show that the equilibrium between $[MoO_3(NTA)]^{3-}$

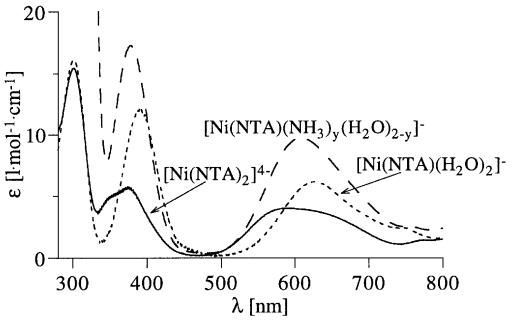

FIG. 4. UV–VIS spectra of Ni–NTA complexes in aqueous solution.

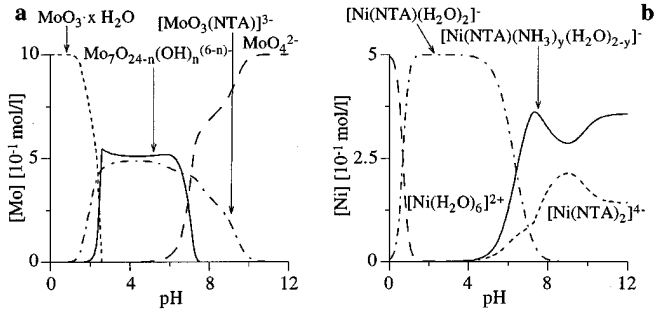

FIG. 5. Thermodynamic predictions of the (a) Mo and (b) Ni species in a 5 mol/l ammonia solution as a function of the pH ($[Mo]_{tot} = 1$ mol/l, Ni : Mo : NTA = 0.5 : 1 : 1).

and $[Ni(NTA)(H_2O)_2]^-$ is on the right-hand side for all pH values ≥ 1:

$$7\,[Ni(H_2O)_6]^{2+} + 7\,[MoO_3(NTA)]^{3-} \rightleftharpoons 7\,[Ni(NTA)(H_2O)_2]^- + Mo_7O_{24}^{6-} + 6H_3O^+ + 19H_2O$$

Therefore, all Ni^{2+} ions are complexed to at least one NTA ligand, and the fraction of Mo present as $[MoO_3(NTA)]^{3-}$ is never larger than 0.5. In agreement with this prediction, the Raman spectrum of a solution containing Ni, Mo, and NTA ions in the ratio 0.5 : 1 : 1 was a superposition of the spectra of $Mo_7O_{24}^{6-}$ and $[MoO_3(NTA)]^{3-}$ (Fig. 2, spectrum II), and the addition of Mo to an acidic $[Ni(NTA)(H_2O)_2]^-$-containing solution did not change its UV–VIS spectrum.

Since $[MoO_3(NTA)]^{3-}$ is not stable in basic solutions (Fig. 1b), an additional NTA molecule becomes available for coordination to Ni above pH = 6 and $[Ni(NTA)_2]^{4-}$ starts to form (Fig. 5). UV–VIS spectra confirmed that a Ni : Mo : NTA solution free of NH_3 and NH_4^+ contained only $[Ni(NTA)\ (H_2O)_2]^-$ at pH = 6.0, and $[Ni(NTA)_2]^{4-}$ at pH = 9.0. However, these two species could not be distinguished by their Ni *K*-edge EXAFS spectra (Fig. 6). The first coordination spheres of these complexes mainly differ by the presence of an oxygen instead of a nitrogen atom, although the coordination distances are similar, as was shown for crystalline $K[Co(NTA)(H_2O)] \cdot 2H_2O$ (18) and $K_4Ni(NTA)_2 \cdot 8H_2O$ (19). Therefore only slight differences will appear in the EXAFS spectra, because the backscattering amplitudes and phase shifts of oxygen and nitrogen are similar (20).

Impregnated Ni–Mo–NTA Catalysts

UV–VIS, IR, and EXAFS measurements proved that, after impregnation of a silica or alumina support with a Ni and NTA containing, or Ni, Mo, as well as NTA containing solution and drying of the resulting samples, the NTA molecules remained complexed with the Ni ions as in the impregnating solutions, but that the ammonia ligands exchanged for OH groups of the support surface. Thus, the UV–VIS reflectance spectra of Ni(NTA)/SiO_2 (4.6 wt% Ni, 15.0 wt%

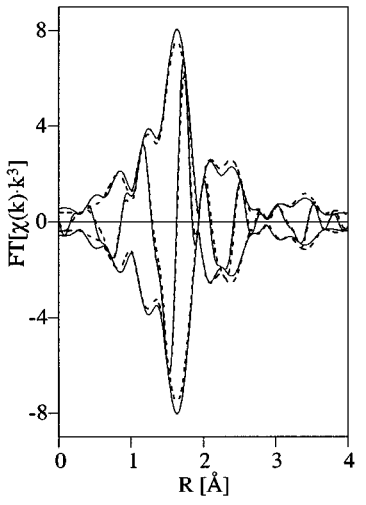

FIG. 6. Fourier transforms of the Ni *K*-edge $\chi(k) \cdot k^3$ for an acid (—) and a basic (- - -) Ni–Mo–NTA (0.5 : 1 : 1) solution.

NTA) and Ni/SiO_2 (2.64 wt% Ni) catalysts (Fig. 7a) resembled those of their impregnation solutions. The spectrum of the Ni/SiO_2 catalyst had maxima at 393 and 674 nm and a shoulder at 750 nm, and is very similar to that of a Ni/SiO_2 catalyst prepared through ion exchange by Bonneviot *et al.* (21). They contacted $[Ni(NH_3)_6]^{2+}$ with SiO_2 and observed that the NH_3 ligands were partly substituted by SiO^- groups of the SiO_2 surface. At the same time, the color changed from purple blue to light green, as with our Ni/SiO_2 catalyst. We therefore conclude that after impregnation of SiO_2 with an ammoniacal solution of $Ni(NO_3)_2$ at pH = 7.5 and drying at 393 K, $Ni(H_2O)_2(NH_3)_2(SiO)_2$ surface complexes are formed. The spectra of the Ni(NTA)/SiO_2 and Ni(NTA)/γ-Al_2O_3 (3 wt% Ni, 9.9 wt% NTA) catalysts showed maxima around 396 and 642 nm and a shoulder at 750 nm (Figs. 7a and 7b), and are very similar to the spectrum of $[Ni(NTA)(H_2O)_2]^-$ in the impregnating solution (Fig. 4). The shifts towards higher wavelength could be due to exchange of some of the NH_3 or H_2O ligands of

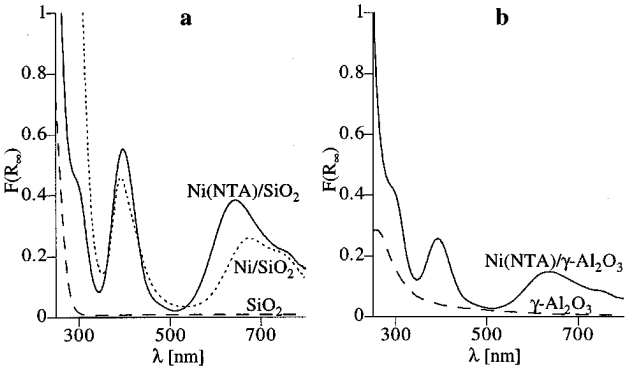

FIG. 7. Reflectance UV–VIS spectra of oxidic Ni catalysts supported on SiO_2 (a) and γ-Al_2O_3 (b).

the $[Ni(NTA)(NH_3)_y(H_2O)_{2-y}]^-$ ($y = 1$ or 2) complexes for surface groups of the supports, as observed for the Ni/SiO_2 catalyst prepared from $[Ni(NH_3)_6]^{2+}$ (21). As in the NTA-free samples, the color of the NTA samples supported on SiO_2 as well as on γ-Al_2O_3 changed from blue to green after drying at 393 K, independent of the Ni : Mo : NTA ratio.

Ni–Mo–NTA catalysts also showed the ligand-exchange effect. Three SiO_2-supported catalysts with the same metal loadings and Ni : Mo : NTA = 0.5 : 1 : 1 ratios, but which were prepared from impregnation solutions with pH varying from 6.0 to 9.0, exhibited the same absorption maximum around 643 nm, although the Ni species in the impregnation solutions were different (mainly $[Ni(NTA)(H_2O)_2]^-$ at pH = 6.0, $[Ni(NTA)(NH_3)_2]^-$ at pH = 7.5, and a mixture of $[Ni(NTA)(NH_3)_2]^-$ and $[Ni(NTA)_2]^{4-}$ at pH = 9.0). This ligand exchange was common to all catalysts containing NTA as a ligand; it was independent of the support (SiO_2 or γ-Al_2O_3), the Ni : Mo ratio, and the pH of impregnation.

Even a $NiMo(NTA)/SiO_2$ 0.3 : 1 : 1 catalyst which was prepared with a solution containing $[Ni(NTA)_2]^{4-}$ exhibited a ligand-exchange effect, since it had a UV–VIS band nearly identical to that of a $Ni(NTA)/SiO_2$ catalyst which had been made from a solution containing $[Ni(NTA)(H_2O)_2]^-$. In fact, the absorption maxima of the catalysts were at 639 and 645 nm, respectively, whereas they were at 585 and 628 nm for the $[Ni(NTA)_2]^{4-}$ and $[Ni(NTA)(H_2O)_2]^-$ complexes in solution, respectively (17). This suggests that also the $[Ni(NTA)_2]^{4-}$ complex replaces one or more of its ligands with SiO^- groups. In agreement with this explanation, a typical feature of $[Ni(NTA)_2]^{4-}$, a strong IR band at 1730 cm^{-1} due to the free acetate groups (22), was not observed in any of our catalyst samples. Evaporation of NH_3 during the drying at 393 K and the subsequent decrease of the pH on the support surface may cause the decomposition of this complex in a free NTA molecule and $[Ni(NTA)(H_2O)_2]^-$, since $[Ni(NTA)_2]^{4-}$ is only stable in neutral and basic aqueous solutions (Fig. 3).

The transmission IR spectra of the NiMo(NTA) catalysts supported on SiO_2 and on γ-Al_2O_3 (Fig. 8) corroborate the above conclusions. For catalysts containing Ni as well as Mo, the CO stretching vibration of the NiMo(NTA) catalysts smoothly shifts with increasing Ni : Mo ratio from 1660 cm^{-1} for $Mo(NTA)/\gamma$-Al_2O_3 and 1640 cm^{-1} for $Mo(NTA)/SiO_2$ to 1600 cm^{-1} for the $NiMo(NTA)/SiO_2$ and $NiMo(NTA)/\gamma$-Al_2O_3 0.5 : 1 : 1 catalysts, which is the same value as for the Ni(NTA) catalyst and the $[Ni(NTA)(H_2O)_2]^-$ complex (22). This demonstrates that NTA preferentially binds to the Ni centers in the NiMo catalysts.

The Ni *K*-edge spectra of the NTA-containing catalysts supported on SiO_2 and γ-Al_2O_3 measured at about 130 K hardly differed from those of the solutions measured at room temperature, confirming that the Ni^{2+} environment in the dried, oxidic catalysts resembles very much that in the $[Ni(NTA)(H_2O)_2]^-$ or $[Ni(NTA)_2]^{4-}$ complexes. This

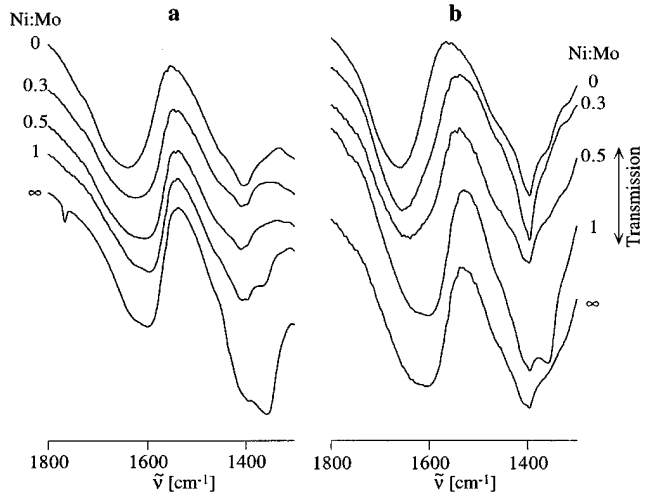

FIG. 8. Transmission IR spectra of oxidic (a) $NiMo(NTA)/SiO_2$ and (b) $NiMo(NTA)/\gamma$-Al_2O_3 catalysts as a function of the Ni : Mo ratio, at a Mo : NTA = 1 : 1 ratio.

is in agreement with the IR and UV–VIS measurements which showed that the Ni^{2+} ions are still complexed by NTA after bringing the impregnation solutions in contact with the supports. The first peak in the Mo EXAFS spectrum of the $NiMo(NTA)/SiO_2$ 0.5 : 1 : 1 catalyst was smaller than that of the $Mo(NTA)/SiO_2$ catalyst (Fig. 9), indicating that the neighbors of Mo are on average less well ordered in the $NiMo(NTA)/SiO_2$ catalyst. This is in agreement with the UV–VIS and IR results which showed that in the $NiMo(NTA)/SiO_2$ catalyst about half of the Mo is present as $[MoO_3(NTA)]^{3-}$ and the other half as polymolybdate. The second shell around 3 Å is absent in the spectrum of the $Mo(NTA)/SiO_2$ catalyst (Fig. 9), confirming that polymolybdates are only present when Ni ions are

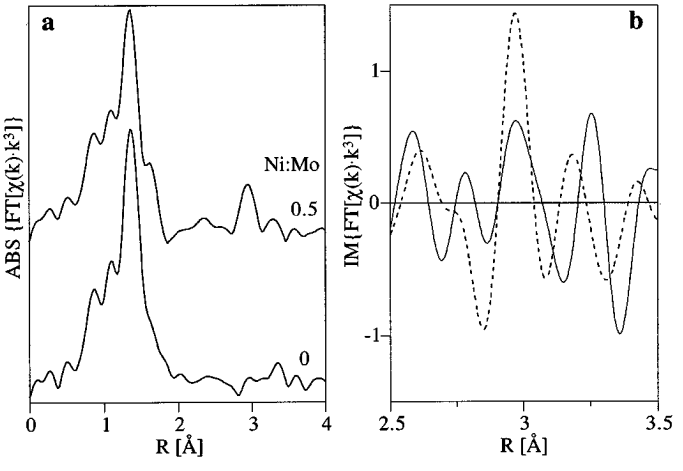

FIG. 9. Absolute (a) and imaginary (b) parts of the Fourier transforms of the $\chi(k) \cdot k^3$ Mo *K*-edge EXAFS of $Mo(NTA)/SiO_2$ 1 : 1 (—) and $NiMo(NTA)/SiO_2$ 0.5 : 1 : 1 (- - -) catalysts.

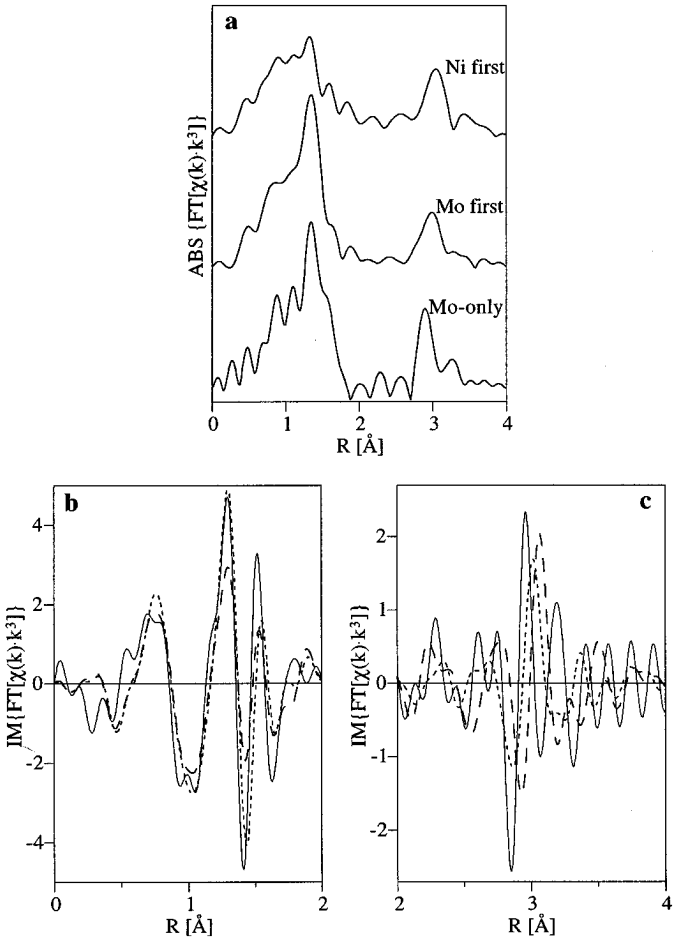

FIG. 10. Absolute (a) and imaginary (b, c) parts of the Fourier transforms of the $\chi(k) \cdot k^3$ Mo *K*-edge EXAFS of two dried NiMo/SiO_2 0.5 : 1 catalysts, Mo-first (- - -) and Ni-first (– – –), and of a Mo/SiO_2 catalyst (—).

present in the (Mo : NTA = 1) impregnation solution. The second peak of the NiMo(NTA)/SiO_2 0.5 : 1 : 1 catalyst is smaller than that of the Mo/SiO_2 catalyst (Fig. 10), but has the same phase shift. Quantitative analysis of the isolated second peak ($2.55 \leq R \leq 3.37$ Å) showed that this peak is a superposition of a small Mo–Mo contribution at 3.3 Å and of a Mo–Si contribution (1.5 neighbors) at 3.5 Å (Table 2), just as for the Mo/SiO_2 catalyst.

Impregnated Ni–Mo Catalysts

For comparison with the NTA-containing Ni–Mo catalysts, NiMo/SiO_2 catalysts which do not contain chelating ligands and which were not calcined during preparation were investigated as well. Their colors and UV–VIS absorption spectra (Fig. 11) were different from those of the NTA-containing catalysts. The co-impregnated, Mo-first and Ni-first catalysts were pale yellow, whereas the Mo-first catalyst prepared at pH ≈ 5.5 was orange-brown. The absorption maxima were lower and were shifted toward higher

TABLE 2

Coordination around Mo in Its Second Coordination Shell in the Mo/SiO_2, NiMo/SiO_2 (Mo first), NiMo/SiO_2 (Ni first), and NiMo(NTA)/SiO_2 Catalysts (Ni : Mo = 0.5 : 1)

Catalyst	Shell	N_{coord}	R [Å]	$\Delta\sigma^2$ [Å^2]	ΔE_0 [eV]
Mo-only	Mo	0.6	3.29	0.0001	1.8
	Si	1.6	3.5	0.0027	−8.1
Mo first	Mo	0.4	3.32	0.0013	0.8
	Si	1.9	3.46	0.0048	−10.8
Ni first	Ni	1.2	3.28	0.0012	−9.1
NTA	Mo	0.4	3.3	0.0001	−2.8
	Si	1.5	3.5	0.0069	−13.1

wavelengths compared to the NTA-containing catalysts. Although ammoniacal solutions were used during preparation of the NiMo/SiO_2 catalysts, the high wavelengths of the absorption bands (690 nm for the Ni-first, and 712 nm for the co-impregnated and Mo-first NiMo/SiO_2 catalysts) indicate that almost no Ni-ammine complexes were present after drying. $[Ni(H_2O)_6]^{2+}$ has a weak and broad maximum around 720 nm, while $[Ni(NH_3)_n(H_2O)_{6-n}]^{2+}$ complexes have maxima around 600 nm. The same phenomenon was observed for the γ-Al_2O_3-supported catalysts: the maximum in the UV–VIS absorption curve shifted from 600 nm for the $[Ni(NH_3)_n(H_2O)_{6-n}]^{2+}$ solution ($n = 3$–6) to 674 nm after drying at 393 K, and shifted further to 700 nm after calcination. Apparently, NH_3 evaporates during drying and calcining of NiMo/SiO_2 and NiMo/Al_2O_3 catalysts, leaving behind Ni ions which are exclusively coordinated by oxygen, either from H_2O, OH^-, O^{2-}, SiO^-, or AlO^-.

In order to better study the Ni and Mo structures of the oxidic NiMo/SiO_2 catalysts, EXAFS spectra were measured. The first shell oxygen coordination around Mo in many oxidic compounds, including the $[MoO_3(NTA)]^{3-}$

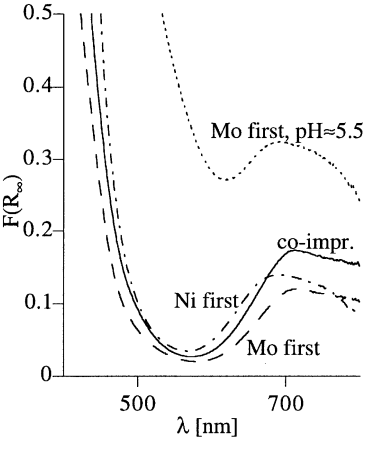

FIG. 11. Reflectance UV–VIS spectra of dried NiMo/SiO_2 catalysts.

complex (23), is strongly distorted. The same is true for the Ni coordination in the $[Ni(NTA)(H_2O)_2]^-$ and $[Ni(NTA)_2]^{4-}$ complexes. This makes a quantitative analysis of their first coordination shells almost impossible, since due to the short data range of light backscattering elements like oxygen and nitrogen and the spread in the distances, EXAFS underestimates coordination numbers at an average value of the real coordination distances and overestimates the disorder (24). For these reasons we have refrained from performing quantitative analyses of the *first* coordination shells around the Ni and Mo centers.

In the Fourier transformed Ni EXAFS spectrum of the $NiMo/SiO_2$ 0.5 : 1 (Ni-first) catalyst a peak was present at 2.7 Å due to atoms in the *second* coordination shell (Fig. 12). This peak was neither present in the spectrum of the $NiMo(NTA)/SiO_2$ 0.5 : 1 : 1 catalyst, nor in that of the $NiMo/SiO_2$ 0.5 : 1 (Mo-first) catalyst. The filtered data of this peak (the inverse Fourier transformation range was $2.27 \leq R \leq 3.35$ Å) could be fitted with 4.7 Ni neighbors at 3.12 Å ($\Delta\sigma^2 = 0.0016$ Å^2, $\Delta E_0 = -3.5$ eV). The fit passed the statistical F-test at the 95% level (the regression square sum was compared with the residual square sum, used as an estimate of the standard deviation of the data (25)). The peak might therefore be due to the presence of $Ni(OH)_2$, because in this compound Ni has 6 Ni neighbors at 3.13 Å (26). Some peaks at larger distances, matching those of crystalline $Ni(OH)_2$, were also found. Their low intensities indicate that the $Ni(OH)_2$ is poorly dispersed on the SiO_2 surface.

The Mo K-edge EXAFS of the $NiMo/SiO_2$ 0.5 : 1 catalysts is strongly influenced by the impregnation order of the Ni and Mo salts (Fig. 10). In the absolute part of the Fourier transformed spectrum of the Mo/SiO_2 catalyst, the asymmetry of the first Mo–O coordination at 1.4 Å and the two intense sidelobes at lower distances (Fig. 10a) testify that the Mo atoms are in a strongly distorted environment typical for oxidic Mo samples. When Mo is impregnated first in the $NiMo/SiO_2$ catalyst preparation, the arrangement of the nearest neighbors around Mo is nearly identical with that in Mo/SiO_2, whereas the inverse contacting order leads to a different first Mo coordination shell. The phases of all three samples are nearly the same in the range between 0.8 and 1.8 Å, indicating that Mo is always in contact with the same type of atom, e.g., oxygen (Fig. 10b).

The second peak at about 3 Å of the Fourier-transformed Mo EXAFS signal also depends on the preparation procedure. Its intensity for the Mo/SiO_2 catalyst (Fig. 10a) is similar to that of oligomeric clusters of MoO_3 (24, 27), but, because the Mo/SiO_2 catalyst was only dried and not calcined, the peak could also be due to polymolybdates which are known to possess several Mo–O and Mo–Mo distances of about 3 Å. The second shell contributions were Fourier filtered in order to gain information about the nature of the neighbors. The fitting procedure delivered the parameters listed in Table 2 and the results shown in Fig. 13. One contribution in the spectrum of the Mo/SiO_2 catalyst was attributed to 0.6 Mo at 3.29 Å, the other to 1.6 Si neighbors at 3.50 Å. Unfortunately, the usual procedure of fitting at the same time in the k^1- and k^3-spaces could not be applied to this sample, because the amplitude of the sidelobe at 3.25 Å could not properly be fitted simultaneously in the k^1- and k^3-Fourier-transformed spectra. Therefore, the fit was performed on the $\chi(k) \cdot k^1$ data only. The number of degrees of freedom was large enough to perform an F-test. The total fit is statistically significant.

The second peak in the Fourier transformed spectrum of the $NiMo/SiO_2$ (Mo-first) catalyst is mainly determined by Si neighbors, because the $\chi(k) \cdot k^3$ function has a maximum at 8 Å^{-1} and decreases rapidly above 10 Å^{-1} (Fig. 13c) (20). A good fit was obtained with Mo–Si as well as Mo–Mo contributions (Table 2). The coordination numbers and distances were similar to those of the Mo/SiO_2 sample, but the Debye–Waller factors were much larger. When the impregnation order was reversed, $\chi(k) \cdot k^3$ had an envelope characteristic for 3d backscatterers with a maximum around 10 Å^{-1} (20). The best fit was obtained with 1.2 Ni neighbors at 3.28 Å (Table 2). The agreement of the absolute value between raw data and fit is not very good (Fig. 13d), probably due to the presence of small Mo–Mo contributions. An additional coordination shell could not be added to the fit, however, because the data have only 4.6 degrees of freedom (the reliability range of the Mo–Ni reference extends from 3.5 to 16.11 Å^{-1}). It may seem surprising that this Mo–Ni coordination was not observed in the Ni EXAFS. The low data quality above 11 Å^{-1}, the region where the Mo scattering power is highest compared to Ni, Si, and O (20), and the large Ni–Ni peak at 3.12 Å, which may overshadow the small Ni–Mo contribution, are possible explanations.

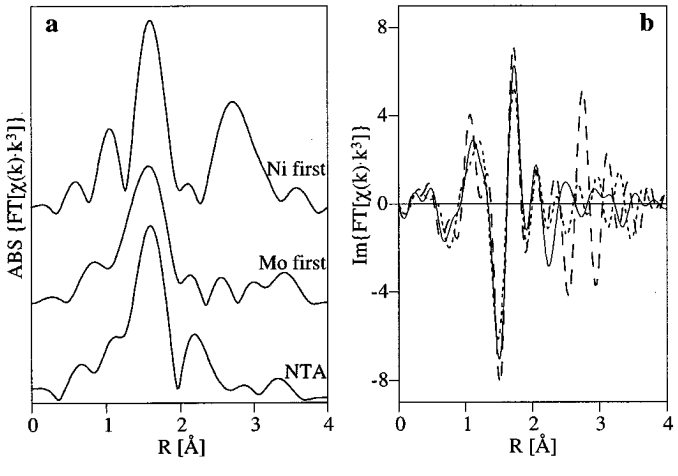

FIG. 12. Absolute (a) and imaginary (b) parts of the Fourier transforms of the $\chi(k) \cdot k^3$ Ni K-edge EXAFS of two dried $NiMo/SiO_2$ 0.5 : 1 catalysts, Mo-first (- - -) and Ni-first (– – –), and of a $NiMo(NTA)/SiO_2$ 0.5 : 1 : 1 catalyst (—).

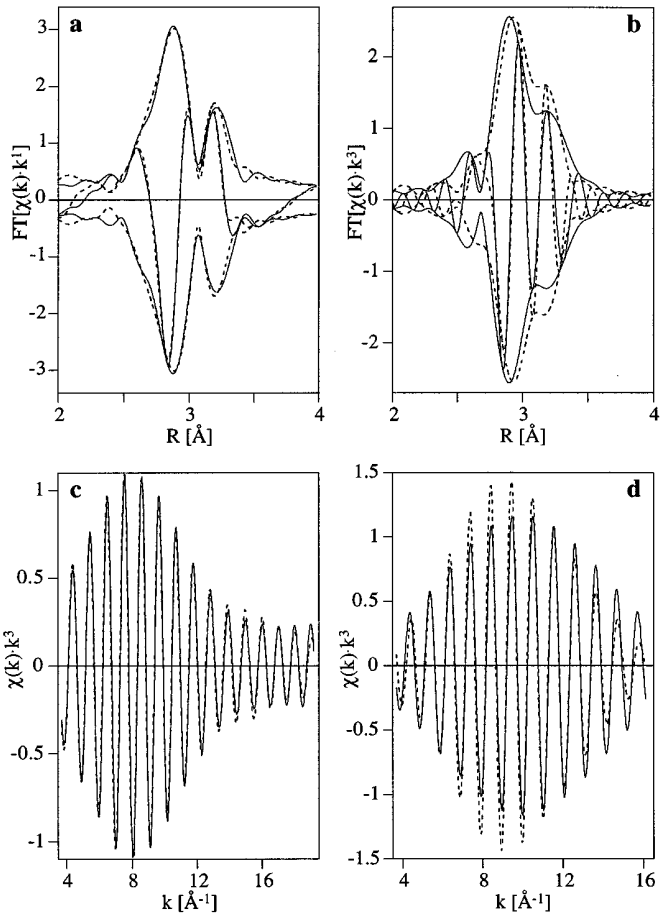

FIG. 13. Fits of the second shells of Mo *K*-edge $\chi(k)\cdot k^1$ (a) and $\chi(k)\cdot k^3$ (b) Fourier transforms of the dried Mo/SiO_2 catalyst, and of $\chi(k)\cdot k^3$ of the NiMo/SiO_2 (0.5 : 1) Mo-first (c) and Ni-first (d) catalysts; curves are filtered data (—) and fit (- - -).

DISCUSSION

Impregnating Solutions

The Raman and UV–VIS spectra clearly demonstrated that, as predicted by the thermodynamic data, the stability of the $[MoO_3(NTA)]^{3-}$ complex in solution is lower than that of $[Ni(NTA)(H_2O)_2]^-$. When the Ni : NTA ratio is smaller than one, the remainder of the NTA which is not bound to Ni ions complexes to a large extent with Mo ions in the pH range 2–8. For a solution containing Ni, Mo, and NTA in the ratio 0.5 : 1 : 1 this means that all Ni ions are complexed with NTA, and that about half of the Mo ions are complexed with NTA. The remaining Mo is present as heptamolybdate or molybdate anions.

We have found no evidence for the formation of a binuclear Ni–Mo–NTA complex in solution. Such a complex was proposed by van Veen *et al.* (4) to explain the beneficial effect of NTA on the catalyst performance. In particular, the $[Ni(NTA)_2]^{4-}$ complex, with its two free acetate functions, would be a likely candidate for the formation of binuclear NiMo complexes. Particularly this complex, however, is the least stable Ni complex and loses an NTA molecule when impregnated on SiO_2 and dried.

Impregnated Ni–Mo–NTA Catalysts

The Ni environment did not change much after impregnation of the SiO_2 or γ-Al_2O_3 support with the Ni–Mo–NTA solution and successive drying. The UV–VIS reflectance and Ni *K*-edge EXAFS spectra demonstrated that Ni^{2+} is always in a similar environment in the NTA-based catalysts, independent of the support (SiO_2 or γ-Al_2O_3) and of the Ni : Mo and Ni : NTA ratios. Whereas the UV–VIS measurements only allowed one to analyze the Ni^{2+} coordination, the IR-active ν(C–O) stretching vibration of the COOM group is also sensitive to the Mo(VI) environment. The IR results agreed well with the UV–VIS data, because when the Ni : Mo ratio increased, the position and the shape of the band due to the ν(C–O) COOM vibration grew more similar to that of the Ni(NTA)/SiO_2 or Ni(NTA)/γ-Al_2O_3 catalysts and no longer resembled that of the corresponding Mo samples. This confirms that NTA preferentially binds to Ni rather than to Mo.

The complexes of Ni^{2+} with NTA exchange one or two of the more labile ligands (H_2O or HN_3) for SiO^- and AlO^- surface groups upon deposition on the oxidic support and successive drying, because it was observed that during this procedure the UV–VIS absorption band at 625 nm of the $[Ni(NTA)(H_2O)_2]^-$ complex shifted toward 642–645 nm. That no Ni–Si or Ni–Al coordination at ca. 3.3 Å was found by EXAFS in the NiMo catalysts might be due to overlap with the contribution of the carbonyl oxygen atoms of the NTA acetate groups (cf. Fig. 6) and to a spread in these Ni–Si and Ni–Al distances.

The $[Ni(NTA)_2]^{4-}$ complex does not seem to be stable in the oxidic catalyst precursors, because a shift of its absorption maximum from 585 to 639 nm upon impregnating SiO_2 with a $[Ni(NTA)_2]^{4-}$ containing solution and drying of the resulting catalyst precursor is too large to be explained by the exchange of only one or two acetate groups of the complex for SiO^- surface groups. Its decomposition upon impregnation and drying could be due to a decrease of the pH in the pores, partly caused by the buffer capacity of the SiO_2 surface and partly by the evaporation of NH_3 during the drying procedure (as Fig. 3 shows, $[Ni(NTA)_2]^{4-}$ is only stable under basic conditions). Unfortunately, the decomposition of the complex could not be confirmed by EXAFS, because the spectra of the $[Ni(NTA)(H_2O)_2]^-$ and $[Ni(NTA)_2]^{4-}$ complexes were equal. Clause *et al.* (28) also observed the exchange of one ethylenediamine (en) ligand of the $[Cu(en)_2(H_2O)_2]^{2+}$ complex for two SiO^- groups during the grafting of the Cu^{2+} ion upon drying at 393 K in an ion-exchanged Cu(en)$_2$/SiO_2 sample.

Although it is known that Mo(VI) ions have a very weak interaction with the SiO_2 surface independent of the pH of

the Mo(VI)-containing solution and that, therefore, bulk MoO_3 is already produced at low Mo loading after high temperature calcination (27, 29–31), the second coordination peak in the Mo EXAFS Fourier transforms was always small, indicating that the dispersion of the Mo species after drying (but no calcination) is quite good (Figs. 9 and 10). The structure around Mo in the NTA-based SiO_2-supported dried catalyst precursors depends on the Ni : Mo ratio. Mo is very well dispersed in the Mo(NTA)/SiO_2 catalyst, since no higher shells were observed above 3 Å. When Ni is added to the Mo- and NTA-containing impregnation solution, the contributions around 3 Å in the Mo *K*-edge EXAFS data (Fig. 10) are mainly due to Mo and Si neighbors (Table 2). A Mo–O–Si coordination has been reported in Raman studies of a catalyst made by impregnation of SiO_2 with aqueous $(NH_4)_6Mo_7O_{24}$ solutions at pH = 7, subsequent high temperature treatment at 773 K in air, and exposure to (wet) air (30–32). EXAFS studies of well-dispersed calcined Mo/SiO_2 samples made from $MoCl_6^{3-}$, and which had been exposed to air, on the other hand, showed three Mo–Mo shells between 3.37 and 3.61 Å, but no Mo–Si interaction (27).

The Mo–Si and Mo–Mo distances measured in the present study agree well with those of crystalline 12-molybdosilicic acid (33), but the Mo–Si coordination numbers were always too high, and the Mo–Mo coordination numbers too small for Mo atoms in the $[SiMo_{12}O_{40}]^{4-}$ Keggin-type structure (Table 2). Since the fitted coordination numbers may contain a large error due to their small contribution to the overall EXAFS signal (Figs. 9 and 10), and the Mo–Si coordination is most probably overestimated by the theoretical FEFF reference (10, 34), fragments of 12-molybdosilicic acid may indeed be present on the surface of the dried catalyst precursors. Rocchiccioli-Deltcheff *et al.* (30) have proposed that Mo_3O_{13} trimolybdic groups may form on the silica surface, randomly connected to each other and to the silica through Mo–O–Si bonds. Some trimolybdic groups could grow together into the 12-molybdosilicic $[SiMo_{12}O_{40}]^{4-}$ structure. Such structures might be in accordance with our EXAFS results.

Impregnated Ni–Mo Catalysts

The Ni and Mo environments in the NiMo/SiO_2 catalysts made by sequential impregnation depend very much on the order of impregnation and are different from the NTA-based counterparts, as shown by their UV–VIS (Fig. 11) and EXAFS spectra (Figs. 10 and 12). When Mo was added first to the SiO_2 support, neither $Ni(OH)_2$ nor Ni silicates were observed in the Ni EXAFS measurements (Fig. 12). The absence of higher coordination shells in the Fourier transformed data and the similarities of the XANES and EXAFS spectra with those reported by Clause *et al.* (35) for crystallized $Ni(NO_3)_2$ suggest that the Mo-covered SiO_2 surface has a buffer capacity which is large enough to decrease the pH of the Ni^{2+} solution in the pores below 6, and thus may hinder the precipitation of $Ni(OH)_2$ as well as the formation of Ni silicates.

When Ni was added first to the SiO_2 support, the second peak in the pseudo-radial distribution at the Ni *K*-edge, which is attributed to Ni neighbors at 3.12 Å, was very strong. $Ni(OH)_2$ (25), Ni nepouite, and Ni talc (36) possess such Ni–Ni distances. Ni nepouite and Ni talc also have a Ni–Si coordination shell at ca. 3.25 Å (37) which could not be found in the NiMo/SiO_2 (Ni-first) catalyst. We therefore conclude that $Ni(OH)_2$ precipitates on the surface of the Ni-first catalyst, as found from acoustophoresis studies on Co(II) solutions contacted with SiO_2 (29), instead of forming a Ni silicate. Since the presence of a free SiO_2 surface seems to be essential for the formation of Ni–Ni interactions, it is nevertheless possible that some linkages of $Ni(OH)_2$ with the surface of the support exist but could not be detected in the Ni EXAFS spectrum. It may even be that a surface Ni silicate is formed during this process, but that the stacking of the SiO_2 and $Ni(OH)_2$ layers is still absent. Further investigations are needed to clarify this point.

The first Mo neighbors are more disordered in the dried NiMo/SiO_2 (Ni-first) catalyst than in the other catalysts, independent of the presence of Ni and NTA, since the amplitude of the first peak of the Fourier transformed Mo *K*-edge spectrum is smallest for this sample (Figs. 9a and 10a). Compared with the Mo/SiO_2 catalyst, the second peak of the NiMo/SiO_2 (Ni-first) catalyst is less intense, shifted towards larger distances, and its imaginary part is different (Fig. 10a). The best fit was obtained with a Ni contribution at 3.28 Å.

This information leads to the following model for the preparation of the NiMo/SiO_2 (Ni-first) catalyst. In the first impregnation step, Ni^{2+} is adsorbed on the SiO_2 support and builds small $Ni(OH)_2$ crystallites. The second impregnation solution contains MoO_4^{2-} ions which feel repulsive interactions with the free SiO_2 surface, since SiO_2 has a point of zero charge (PZC) of pH ≈ 2.0 and is thus covered with SiO^- groups. However, the surface of the $Ni(OH)_2$ crystallites is positively charged, since its PZC is much higher ($Co(OH)_2$ has a PZC of pH ≈ 11.0 (38)). An attractive interaction between $Ni(OH)_2$ ad MoO_4^{2-} during the second impregnation step explains the formation of the Mo–Ni coordination after drying at 393 K. The adsorption of Mo on the surface of the $Ni(OH)_2$ particles may also be responsible for the stronger distortion of the first Mo–O shell compared with the other catalysts. As a consequence, the dispersion of the Mo species is very high and Mo–Mo interactions in the oxidic catalyst precursor are small.

For the NiMo(NTA)/γ-Al_2O_3 0.5 : 1 : 1 (2.64 wt% Ni, 8.64 wt% Mo, and 17.21 wt% NTA) catalyst, the same conclusions regarding the Ni-environment as for its SiO_2 counterparts can be drawn from the similar UV–VIS and EXAFS Ni *K*-edge results. In contrast, the Ni atoms in the calcined

NiMo/γ-Al_2O_3 0.5 : 1 catalyst (with the same metal loadings as for the NTA sample) are in a different environment than Ni atoms in the SiO_2-supported catalysts dried at 393 K. $Ni(OH)_2$ and NiO can be excluded because of the absence of higher neighboring shells, whereas $Ni(NO_3)_2$ cannot be formed because of the high temperature treatment. Analogously to the Mössbauer emission spectroscopy results of Wivel *et al*. (39) on CoMo/γ-Al_2O_3 catalysts, it is concluded that in this sample Ni is very well dispersed in octahedral and tetrahedral sites on the γ-Al_2O_3 surface. Mo should be present as a mixture of molybdate, polymolybdates, and well-dispersed MoO_3 crystallites (24, 40).

CONCLUSIONS

The UV–VIS, IR, and EXAFS measurements have shown that the Ni^{2+} ions in the dried, uncalcined NiMo catalyst precursors prepared with the NTA-recipe and supported on either SiO_2 or γ-Al_2O_3 are complexed with NTA. Ni is mainly present as $[Ni(NTA)(H_2O)_2]^-$, independent of the Ni : Mo and Ni : NTA ratios. During drying, NH_3 evaporates and coordinated H_2O is replaced by surface groups of the support. As a consequence of the Ni : Mo : NTA = x : 1 : 1 ratios, Mo is only coordinated to NTA when more NTA than Ni^{2+} is present in the impregnation solution. That part of the Mo which interacts with the SiO_2 surface to form well-dispersed surface molybdates increases with increasing Ni : Mo ratio, and is similar to that in catalysts prepared in the absence of chelating ligands by sequential impregnation of Mo followed by Ni for a Ni : Mo ratio of 0.5. Without calcination, these surface molybdates are grafted on the SiO_2 support by Si–O–Mo bonds.

The catalysts made by sequential impregnation in the absence of NTA have different Ni^{2+} -environments from their NTA counterparts. When Ni is impregnated first, $Ni(OH)_2$ crystallites are formed on the SiO_2 surface, and Mo is attracted by the positive surface of the $Ni(OH)_2$ crystallites during the second impregnation step. Therefore, after drying, a Mo–Ni coordination exists. When the impregnation order is reversed, Mo is well dispersed on the SiO_2 surface by Si–O–Mo bonds and Ni crystallizes as $Ni(NO_3)_2$.

ACKNOWLEDGMENTS

The authors thank Dr. R. Kissner of the Laboratory for Inorganic Chemistry of the ETH Zürich for making an extended version of the program SPEX (41) available, and Dr. E. Blank and Mr. Y. von Känel of the Department of Materials Science of the Swiss Federal Institute of Technology in Lausanne (EPFL) for the Raman measurements.

REFERENCES

1. Zdražil, M., *Catal. Today* **3**, 269 (1988).
2. Prins, R., de Beer, V. H. J., and Somorjai, G. A., *Catal. Rev.-Sci. Eng.* **31**, 1 (1989).
3. Thompson, M. S., European Patent Application 0.181.035, 1986.
4. Van Veen, J. A. R., Gerkema, E., van der Kraan, A. M., and Knoester, A., *J. Chem. Soc., Chem. Commun.* 1684 (1987).
5. Bouwens, S. M. A. M., Prins, R., de Beer, V. H. J., and Koningsberger, D. C., *J. Phys. Chem.* **94**, 3711 (1990).
6. Bouwens, S. M. A. M., Koningsberger, D. C., de Beer, V. H. J., Louwers, S. P. A., and Prins, R., *Catal. Lett.* **5**, 273 (1990).
7. Louwers, S. P. A., and Prins, R., *J. Catal.* **133**, 94 (1992).
8. Van Veen, J. A. R., Colijn, H. A., Hendriks, P. A. J. M., and van Welsenes, A. J., *Fuel Proc. Technol.* **35**, 137 (1993).
9. Medici, L., and Prins, R., *J. Catal.* (1996).
10. Mustre de Leon, J., Rehr, J. J., Zabinsky, S. I., and Albers, R. C., *Phys. Rev. B* **44**, 4146 (1991).
11. Baes, C. F., and Mesmer, R. E., "The Hydrolysis of Cations," pp. 238, 253. Wiley, New York, 1976.
12. Smith, R. M., and Martell, A. E., "Critical Stability Constants," Vol. 6, pp. 77, 439. Plenum Press, New York, 1989.
13. Kula, R. J., and Rabenstein, D. L., *Anal. Chem.* **38**, 1934 (1966).
14. Martell, A. E., and Smith, R. M., "Critical Stability Constants," Vol. 1, pp. 139, 238. Plenum Press, New York, 1974.
15. Fridman, A., Ya., Dyatlova, N. M., and Fridman, Ya. D., *Russ. J. Inorg. Chem.* **14**, 1741 (1969).
16. Jeziorowski, H., and Knözinger, H., *J. Phys. Chem.* **83**, 1166 (1980).
17. Jørgensen, C. K., *Acta Chem. Scand.* **10**, 887 (1956).
18. Battaglia, L. P., Bommartini Corradi, A., and Vidoni Tani, M. E., *Acta Crystallogr. Sect. Struct. Sci. B* **31**, 1160 (1975).
19. Fomenko, V. V., Polynova, T. N., and Porai-Koshits, M. A., *J. Struct. Chem.* **16**, 602 (1974).
20. Teo, B-K., and Lee, P. A., *J. Am. Chem. Soc.* **101**, 2815 (1979).
21. Bonneviot, L., Legendre, O., Kermarec, M., Olivier, D., and Che, M., *J. Colloid. Interface Sci.* **134**, 534 (1990).
22. Rajabalee, F. J. M., *Spectrochim. Acta A* **30**, 891 (1973).
23. Butcher, R. J., and Penfold, B. R., *J. Cryst. Mol. Struct.* **6**, 13 (1976).
24. Kisfaludi, G., Leyrer, J., Knözinger, H., and Prins, R., *J. Catal.* **130**, 192 (1991).
25. Brook, R. J., and Arnold, G. C., "Applied Regression Analysis and Experimental Design," p. 30. Dekker, New York, 1985.
26. Szytula, A., Murasik, A., and Balanda, M., *Phys. Status Solidi B* **43**, 125 (1971).
27. De Boer, M., van Dillen, A. J., Koningsberger, D. C., Geus, J. W., Vuurman, M. A., and Wachs, I. E., *Catal. Lett.* **11**, 227 (1991).
28. Clause, O., Bonneviot, L., Che, M., Verdaguer, M., Villain, F., Bazin, D., and Dexpert, H., *J. Chim.-Phys. Phys.-Chim. Biol.* **86**, 1767 (1989).
29. De Boer, M., Leliveld, R. G., van Dillen, A. J., Geus, J. W., and Bruil, H. G., *Appl. Catal. A* **102**, 35 (1993).
30. Rocchiccioli-Deltcheff, C., Amirouche, M., Che, M., Tatibouët, J.-M., and Fournier, M., *J. Catal.* **125**, 292 (1990).
31. Stencel, J. M., Diehl, J. R., D'Este, J. R., Makovsky, L. E., Rodrigo, L., Marcinkowska, K., Adnot, A., Roberge, P. C., and Kaliaguine, S., *J. Phys. Chem.* **90**, 4739 (1986).
32. Kasztelan, S., Payen, E., and Moffat, J. B., *J. Catal.* **112**, 320 (1988).
33. Feist, M., Molchanov, V. N., Kazanski, L. P., Torchenkova, E. A., Spitsyn, V. I., *Russ. J. Inorg. Chem.* **25**, 401 (1980).
34. Vaarkamp, M., Dring, I., Oldman, R. J., Stern, E. A., and Koningsberger, D. C., *Phys. Rev. B* **50**, 7872 (1994).
35. Clause, O., Kermarec, M., Bonneviot, L., Villain, F., and Che, M., *J. Am. Chem. Soc.* **114**, 4709 (1992).
36. Clause, O., Bonneviot, L., Che, M., and Dexpert, H., *J. Catal.* **130**, 21 (1991).
37. Perdikatsis, B., and Burzlaff, H., *Z. Krist.* **156**, 177 (1981).
38. James, R. O., and Healy, T. W., *J. Colloid. Interface Sci.* **40**, 53 (1972).
39. Wivel, C., Clausen, B. S., Candia, R., Mørup, S., and Topsøe, H., *J. Catal.* **87**, 497 (1984).
40. Payen, E., Grimblot, J., and Kasztelan, S., *J. Phys. Chem.* **91**, 6642 (1987).
41. Martell, A. E., and Motekaitis, R. J., "The Determination and Use of Stability Constants," VCH, New York, 1988.